

Gravity Currents in Non-rectangular Cross-section Channels

Tamar Zemach and Marius Ungarish

Abstract—We consider the propagation of a high-Reynolds-number gravity current at the bottom of a horizontal channel along the horizontal coordinate x . The bottom and top of the channel are at $z = 0, H$, and the cross-section is given by the general $-f_1(z) \leq y \leq f_2(z)$ for $0 \leq z \leq H$. We use a one-layer, Boussinesq, shallow-water (SW) formulation to solve the time-dependent motion produced by release from rest of a fixed volume of fluid from a lock. The dependent variables are the position of the horizontal interface, $h(x, t)$, and the speed (averaged over the area of the current), $u(x, t)$. For a given geometry $f(z)$, the only input parameter in the lock-release problem is the height ratio H/h_0 of ambient to lock. In general, the solution is obtained by a finite-difference numerical code. Analytical results are derived for the initial dam-break slumping motion, and for the long-time self-similar phase. The model is illustrated for various cross-section shapes: power-law ($f(z) = bz^\alpha$, where b, α are positive constants), trapezoidal and circle-segment. The theoretical results are in good agreement with previously-published experimental data.

Index Terms—gravity currents, shallow-water.

I. INTRODUCTION

A gravity current appears when fluid of one density spreads into a fluid of another density and the propagation is, mainly, in the horizontal direction. Gravity currents occur at a variety of scales throughout nature. Examples include oceanic fronts, avalanches, seafloor turbidity currents, pyroclastic flows, and lava flows (see for example [1]). Most studies have focused on the flow of currents which propagate on the flat bottom (or top) of a rectangular channel. However, gravity currents generated and spreading in channels with non-rectangular cross-sections are realistic configurations in nature (e.g., valleys and rivers), buildings, irrigation systems, and industrial fluid-transport infrastructures. It is therefore of both practical and academic importance to understand and model the effects of this geometrical property on the flow.

In the present paper we consider gravity currents in channels with various forms of the cross-sections. Typical non-rectangular channels are shown for example in Fig. 1. Let x be the horizontal coordinate along the channel, y the horizontal coordinate orthogonal to x , and z the vertical coordinate pointing upward. To be specific, the side-walls are given by $y = -f_1(z)$ and $y = f_2(z)$, $0 \leq z \leq H$. We shall see that the flow depends actually on the width function, $f(z) = f_1(z) + f_2(z)$, which is assumed continuous and positive (zero width at 0 and/or H are allowed).

Our investigation uses a one-layer shallow-water (SW), Boussinesq model. The formulation is in terms of the height h of the interface and speed u (averaged over the area of

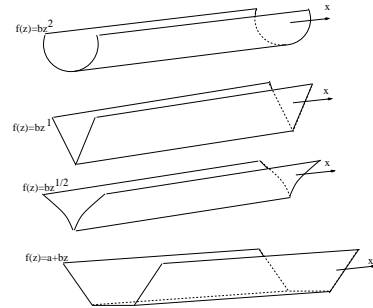


Fig. 1. Schematic description of typical channels with non-rectangular cross-section.

the current) as functions of x and t (time). This allows the calculation of the position of the nose, $x_N(t)$.

The formulation which we derive is applicable to a quite general cross-section function $f(z)$ (the main formal requirement is continuity in $[0, H]$, and the obvious $f(z) > 0$ in $(0, H)$). For definiteness, we shall present results for three types of channels. (A) $f(z) = bz^\alpha$, where b is a positive constant and $0 < \alpha \leq 2$. Experiments for this configuration were presented by [5], for currents released from a full-depth lock. This geometry is referred to as the power-law cross-section. (B) $f(z) = c + bz^\alpha$, where c is a positive constant, and b, α are as above. This geometry is referred to as the curved-trapezoidal cross-section. (C) A circle-sector channel of radius R , $f(z) = \sqrt{2zR - z^2}$, $0 \leq z \leq H < 2R$. The three types of cross-section considered here are interesting from the academic point of view, and their relevance to industrial and environmental applications seems feasible. They cover a quite wide domain of shapes and provide a fair understanding of the effects associated with deviations from the classical rectangular geometry.

The structure of the paper is as follows. In Section II we formulate the model for channels of a general cross-section form. This model includes the shallow-water one-layer equations of motion and the appropriate boundary conditions. We solve this problem numerically in Section III and present detailed time-dependent results for various cross-section channels. In Section IV we concentrate on the analytical solution of the dam-break problem and derive the constant speed of propagation for the initial slumping stage. Next, in Section V, we revisit the analytical similarity solution for the long-time stage of propagation, and compare results with the finite-difference SW solution. In Section VI we compare our SW results with available experimental data, and show that there is fair agreement. In Section VII some concluding remarks are given.

Manuscript received March 21, 2013

T. Zemach is with the Department of Computer Science, Tel-Hai College, Tel-Hai, Israel, e-mail: tamar.zemach@yahoo.com .

M. Ungarish is with Department of Computer Science, Technion, Haifa 32000, Israel, e-mail: unga@cs.technion.ac.il.

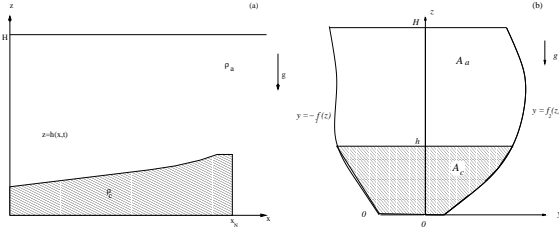


Fig. 2. Schematic description of the gravity current system. (a) Side view. (b) cross-section of channel. Here $f(z)$ is the width of the channel. In the analysis A_a denotes the area occupied by the ambient fluid, $A_c = F(x, t)$ is the area occupied by the current, and A_T is the total area.

II. FORMULATION

The system under consideration is sketched in Fig. 2: a deep layer of ambient fluid of density ρ_a and height H lies above a horizontal surface at $z = 0$. Gravity acts in the $-z$ direction. At time $t = 0$ a given volume of fluid of density $\rho_c > \rho_a$ (the dark region in the figure), initially at rest in reservoir of height h_0 , length x_0 and same cross-section as the channel, is instantaneously released into the ambient fluid. We use a $\{x, y, z\}$ Cartesian coordinate system with corresponding $\{u, v, w\}$ velocity components. We assume that the fluids are separated by a sharp, non-entraining, interface which is flat (horizontal) in the y direction. This is the initial hydrostatic situation in a simple lock. The present model assumes that viscous, turbulent, and entrainment effects are negligible, and hence in the subsequent flow in a straight channel there are no effects that can generate a significant inclination in the y direction.

The driving force is the reduced gravity, which is defined by

$$g' = \epsilon g, \quad (1)$$

where g is the gravitational acceleration and ϵ is the reduced density which is defined by

$$\epsilon = |\rho_c - \rho_a| / \rho_a. \quad (2)$$

We introduce the Boussinesq assumption $\epsilon \ll 1$.

We define $F = F(h)$ to be the cross-section area (also referred to as A_c) occupied by the current

$$F(h) = F(h(x, t)) = \int_0^{h(x, t)} f(z) dz = A_c. \quad (3)$$

Evidently, $F'(h) = f(h)$.

The volume continuity equation of the current can be readily obtained using geometric considerations, see Fig. 2. In the motionless ambient fluid, the pressure does not depend on x . Therefore, the hydrostatic balances $\partial p_i / \partial z = -\rho_i g$, where $i = a$ or c , supplemented by the property of pressure continuity between the ambient and the current on the interface $z = h(x, t)$, show that the horizontal pressure gradient in the current is given by

$$\frac{\partial p_c}{\partial x} = \rho_c g' \frac{\partial h}{\partial x}. \quad (4)$$

The momentum equation of the model is obtained by averaging the inviscid x -momentum balance over the area A_c , and elimination of the pressure term by (4). After some

algebra, and use of (3)-(4), this equation can be reduced to exactly the same form as in the classical rectangular- cross-section case (see below (6)).

It is convenient to use dimensionless variables. Here we denote the dimensional variables by asterisks, and transform to the dimensionless counterpart (with no special notation) as follows:

$$\{x^*, z^*, h^*, H^*, t^*, u^*, p^*\} = \{x_0 x, h_0 z, h_0 h, h_0 H, T t, U u, \rho_a U^2 p\}, \quad (5)$$

where $U = (h_0 g')^{1/2}$ and $T = x_0 / U$. The y -direction lengths are scaled with the width of the interface in the lock, $f(h_0)$.

The resulting dimensionless SW system of equations is

$$\begin{pmatrix} h_t \\ u_t \end{pmatrix} + \begin{pmatrix} u & F(h) \\ 1 & u \end{pmatrix} \begin{pmatrix} h_x \\ u_x \end{pmatrix} = \begin{pmatrix} 0 \\ 0 \end{pmatrix}. \quad (6)$$

The system is hyperbolic, with characteristic relationships given by

$$dh \pm \sqrt{\frac{F(h)}{F'(h)}} du = 0 \quad (7)$$

on

$$\frac{dx}{dt} = c_{\pm} = u \pm \sqrt{\frac{F(h)}{F'(h)}}. \quad (8)$$

For a lock-release problem, the initial conditions are $u = 0$ and given position of the interface (in our case, $h = 1$) in the reservoir. The boundary conditions are: (1) the obvious $u = 0$ at the backwall $x = 0$; and (2) Froude condition at the nose $x = x_N(t)$:

$$u(x = x_N) = u_N = Fr \cdot h_N^{1/2}, \quad (9)$$

where Fr is the Froude number for the appropriate non-rectangular cross-section. As shown by [6], for a given $f(z)$, this reads

$$Fr = Fr_U(\varphi) = \left[\frac{2(1 - \varphi)^2}{1 + \varphi} (1 + Q) \right]^{1/2}, \quad (10)$$

where

$$\varphi = \frac{F(h)}{A_T}, \quad \text{and} \quad Q = \frac{\int_0^h z f(z) dz}{h \cdot [A_T - F(h)]}. \quad (11)$$

Here A_T is the total area of the cross-section, and evidently $\varphi < 1$.

III. FINITE-DIFFERENCE RESULTS

To complete our modelling task, we need an efficient method for obtaining the $h(x, t)$, $u(x, t)$ and $x_N(t)$ results from our formulation. In general, the system of equations (6)-(10), with realistic initial/boundary conditions, cannot be solved analytically. We use a finite-difference two-step Lax-Wendroff method ([9], [10]), To facilitate the implementation of the boundary conditions, the x -coordinate was mapped into the coordinate $\eta = x/x_N(t)$. The SW results displayed here were obtained with, typically, 200 grid points in the $[0, x_N]$ interval, and time step of $1 \cdot 10^{-3}$. (Convergence was tested also on finer grids.)

Some typical results are presented below.

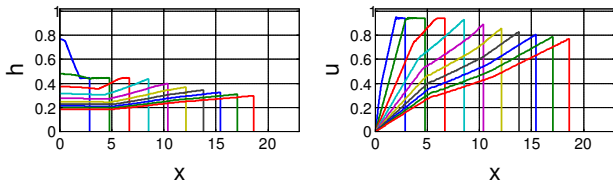


Fig. 3. Profiles of h and u vs. t for various values of t . $H = 20$, $f(z) = z$ for $t = 2(2)20$.

A. Power-law cross-section, $f(z) = bz^\alpha$

The dimensional $f(z) = bz^\alpha$ reads $f(z) = z^\alpha$ in dimensionless form (the scaling width is bh_0^α). This means that the value of b does not influence the results.

The typical behaviour of the time-dependent current is shown in Fig. 3 for $H = 20.0$ and $\alpha = 1.0$.

We can distinguish between three main stages of propagation, like in the classical rectangular geometry. The initial slumping stage is characterized by the constant value of the velocity of the nose u_N , accompanied by a constant value of the nose height h_N . The nose height h_N of the slumping stage increases with α from 0.4 for $\alpha = 0.5$ to about 0.5 for $\alpha = 2$. u_N also increases with α , but more like $h_N^{1/2}$, because Fr is close to a constant ($\approx \sqrt{2}$) for this value of H (not shown here). In the currents under consideration the slumping stage is quite long: until $t \approx 6.4$ for $\alpha = 0.5$, $t \approx 8$ for $\alpha = 1.0$ and $t \approx 12.0$ for $\alpha = 2$. The distance of propagation during this stage increases with α and it attains $x_s \approx 6.4$ for $\alpha = 0.5$, $x_s \approx 8.5$ for $\alpha = 1$, $x_s \approx 11$ for $\alpha = 2$. We conclude that as α increases, the current becomes faster, and the slumping stage becomes longer.

The next stage of propagation is characterized by the decreasing height of the nose and speed. This stage is a transient during which the current approaches a similarity solution. The transition is smooth and it is therefore not possible to give a clear-cut statement when this intermediary phase ends. The long-time profiles display a tendency to self-similar behaviour, which can be identified by a linear dependency of the velocity u on x , and a “tail down - nose up” parabolic form of height h . The similarity solution was reported by [3], [5], and will be discussed in more details in Section V below.

Additional insights were obtained by further comparison with solutions for non-deep ambient $H = 2.0$ (not shown here). Our main conclusion is that the fastest current is obtained for the largest tested α , and the slumping height h_N and distance x_s increase with α .

Fig. 4 illustrates the influence of H on the behaviour of the speed u_N as a function of t for the case $f(z) = z$. The slumping stage of propagation (with constant u_N vs. t) can be clearly seen on the graph. After the slumping stage, there is a clear-cut tendency of the speed to decrease with t , for all H . However, the reduction of speed is not sharp: u_N decays by about 20% while t increases by a factor of more than 3. In other words, in this case u_N decreases less than $t^{-1/5}$.

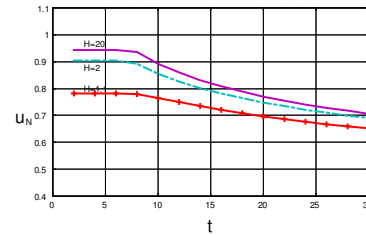


Fig. 4. Numerical results: behaviour of the nose velocity u_N vs. t for $f(z) = z$ and various values of H : 1.1, 2.0, and 20.0. Note the constant velocity.

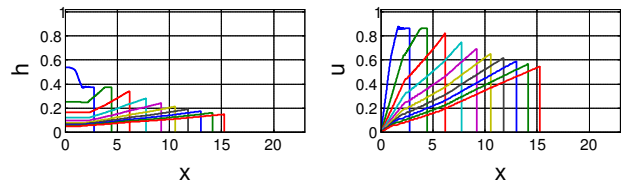


Fig. 5. Profiles of h and u vs. t for various values of t . $H = 20$, $f(z) = (1 + z)/2$ for $t = 2(2)20$

B. Cross-section with $f(z) = c + bz^\alpha$ functions.

The simple (straight planes) trapezoidal case is obtained for $\alpha = 1$. For small values of d we return to the power-law case.

The typical behaviour of the solutions is presented in Fig. 5 for $H = 20.0$ and $f(z) = (1 + z)/2$ (i.e., $d = 1, \alpha = 1$). The current propagation is shown for $t = 2, 4, \dots, 20$.

We tested and compared results for various parameters for the present configuration. In particular, three values of α were used as before 0.5, 1.0, 2.0 and two systems: deep with $H = 20$, and shallow with $H = 2$. For $d = 1$, the main conclusions about the tendency of deep ($H = 20$) currents to propagate faster than non-deep ($H = 2.0$) were similar to these obtained for the $d = 0$ case and described in the previous section. The effect of α on the current is as before: we see faster propagation for larger α .

C. Circle-sector channel ($f(z) = \sqrt{2Rz - z^2}$ function).

Another interesting and practical configuration is the circle-sector channel of radius R .

Here we scale R with h_0 , and, as an exception, we also scale $f(z)$ with h_0 . Therefore, $f(z) = \sqrt{2zR - z^2}$, $0 \leq z \leq H$, and obviously $H < 2R$. A schematic description of this configuration is given in Fig. 6.

The typical profiles of the solutions are presented in Fig. 7 for $H = 20.0$ and $R = 10$. The current propagation is shown for $t = 2, 4, \dots, 20$.

IV. DAM-BREAK AND THE CONSTANT SLUMPING u_N

In general, the shallow-water equations of motion require numerical solution, as illustrated in the previous section. However, some useful analytical results can be obtained for the initial motion after release from rest from behind a straight vertical “dam.”

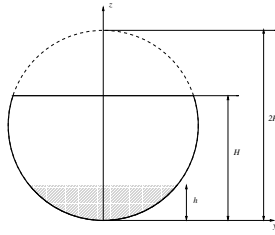


Fig. 6. Circle cross-section $f(z) = \sqrt{2zR - z^2}$

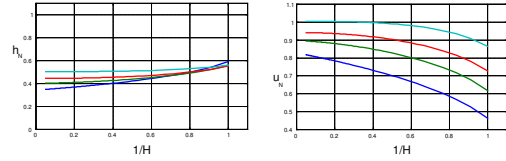


Fig. 8. Analytical results for the slumping stage of the current for $f(z) = z^\alpha$: Nose height and speed as functions of $1/H$. $\alpha = 2$ (light blue online), $\alpha = 1$ (red online), $\alpha = 0.5$ (green online), $\alpha = 0$ (blue online; this is the classical rectangular case).

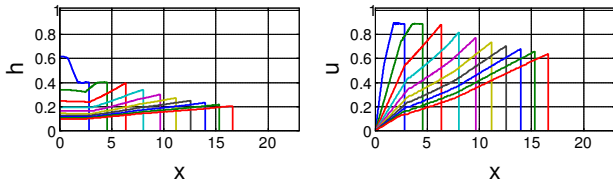


Fig. 7. Profiles of h and u vs. t for various values of t . $H = 20$, $R = 10$, $f(z) = \sqrt{2zR - z^2}$ for $t = 2(2)20$.

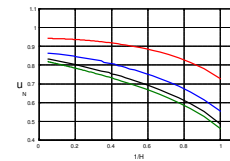


Fig. 9. Analytical slumping speed for trapezoidal $f(z) = (d+z)/(d+1)$, where $d = 0$ (upper line, red online), $d = 1$ (blue online), $d = 5$ (black). The lowest line (green online) is for the classical rectangular cross-section.

We introduce the function

$$\Gamma(h) = \int_0^h \sqrt{\frac{F'(\tilde{h})}{F(\tilde{h})}} d\tilde{h}. \quad (12)$$

The integration of the balance equation (7) for $u(h)$ on a c_+ characteristic from the reservoir to the nose and the intersection of speed dictated by the reservoir, with the nose condition (9) yields:

$$\Gamma(1) - \Gamma(h_N) = Fr(h_N/H) \cdot h_N^{1/2}, \quad (13)$$

where Fr is given by (10). The solution of this algebraic equation provides first h_N , and next u_N .

Analytical slumping results for some typical functions $f(z)$ are presented below.

A. $f(z) = z^\alpha$ (dimensionless)

This case allows some analytical progress. A summary of typical analytical results obtained by the abovementioned calculations are presented in Fig. 8. It displays the nose height h_N and the nose velocity u_N as functions of $1/H$ for four values of α : 0, 0.5, 1.0, 2.0. For $\alpha \geq 0$, u_N increases with H and the nose height h_N decreases with H . It is interesting to note that all the cases considered here display the tendency of an increasing u_N with H . This is consistent with the expectations that a deeper current moves faster.

B. $f(z) = c + bz^\alpha$.

The typical solutions are shown in Fig. 9 for the dimensionless $f(z) = (d+z)/(d+1)$, where $d = 0, 1$ and 5 . The effect of d is interesting: the slumping speed of the current decreases as d increases (for any height of the ambient fluid H). This behavior is, again, in agreement with the numerical SW solutions obtained above (see for example Fig. 3 and Fig. 5). The interpretation is that, for a given h_N , when d is

small, the ratio of A_c to that of the ambient is smaller than in the rectangular case; therefore the current feels thinner, and is faster. The $d = 5$ case is very close to the rectangular cross-section solution.

C. Circle-sector channel

We focus on the $R = 10$ case, and let H vary. Fig. 10 displays the nose height h_N and the nose velocity u_N as functions of $1/H$. Again, the speed u_N , increases with H and the nose height h_N decreases with H . (This means that Fr increases faster than the decrease of $h_N^{1/2}$.)

We mention here that numerical results of the initial-value problem were also obtained for deep ($H = 20$) and shallow ($H = 2$) cases with two values of R : 10 and 20. For the shallow case with $H = 2$ we obtain that the velocity of the current decreases for increasing values of R . For $H = 20$, the numerical results were almost unaffected by these changes of the radius R . In all cases, the finite-difference results were in excellent agreement with the analytical solution during the slumping stage of propagation.

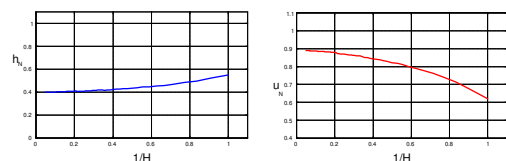


Fig. 10. Analytical slumping results for circle segment $f(z) = \sqrt{2Rz - z^2}$, $0 \leq z \leq H$ and $R = 10$: nose height and nose velocity as functions of $1/H$.

V. SIMILARITY SOLUTIONS

Analytical results of self-similar type are also of importance in the study of gravity currents, and it makes sense to ask how this branch of results is affected by the function $f(z)$.

The accepted argument is that, at large times after release, the current is not influenced by the initial conditions. Moreover, in this stage of propagation, the current is already thin and therefore Fr can be considered as constant ($=\sqrt{2}$ theoretically). In these circumstances, the SW equations are expected to admit a self-similar solution of the form

$$x_N(t) = Kt^\beta, \quad h_N(t, \eta) = (\dot{x}_N)^2 \mathcal{H}(\eta), \quad (14)$$

$$u_N(t, \eta) = \dot{x}_N \mathcal{U}(\eta),$$

where

$$\eta = \frac{x}{x_N}; \quad (15)$$

$$\mathcal{H}(1) = 1/Fr^2; \quad \mathcal{U}(1) = 1. \quad (16)$$

The upper dot means time derivative, and K and β are constants.

The formulation above satisfies the nose condition $u_N = \dot{x}_N = Fr \cdot h_N^{1/2}$. The remaining details must be obtained from the other boundary conditions and the equations of motion.

The extension to the non-rectangular case is, in general, problematic. The Fr approaches the same constant as in the classical case. However, the difficulty appears because the area of the current, $A_c(h)$, is in general not a separable function of t and η . Indeed, [3], [5] have derived, for the SW equations in power-law cross-sections $f(z) = z^\alpha$, similarity solutions of the form (14). The results, in dimensionless form, for a current of fixed volume (dimensionless) $V = 1/(\alpha + 1)$ read

$$\beta = \frac{2 + 2\alpha}{3 + 2\alpha}, \quad (17)$$

$$\mathcal{H}(\eta) = \frac{1}{Fr^2} - \frac{1 - \eta^2}{4(\alpha + 1)}, \quad \mathcal{U}(\eta) = \eta, \quad (18)$$

$$K = \left(\frac{1}{\beta}\right)^\beta \left(\frac{1}{\int_0^1 \mathcal{H}^{\alpha+1}(\eta) d\eta}\right)^{1/(2\alpha+3)}. \quad (19)$$

It can be verified by substitution that this solution satisfies the equations (6).

α	β	K
0	0.667	1.890
0.5	0.750	1.765
1.0	0.800	1.694
2.0	0.857	1.613

TABLE I

SIMILARITY SOLUTION COEFFICIENTS FOR $f(z) = z^\alpha$ CROSS-SECTION

Finally, we verify that the self-similar behavior is indeed attained by the lock-released current. We recall that the finite-difference time-dependent SW solution show the tendency to approach a “nose up - tail down” parabolic h profile, and linear with x profile of u , as seen in Fig. 3 More careful comparisons between the similarity analytical expressions (14) and the finite-difference results are shown in Fig. 11 for $f(z) = z^\alpha$. The values of K, β used in this comparison are given in Table 1.

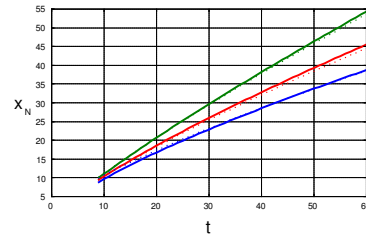


Fig. 11. Comparison between analytical similarity solutions (14) (dots) and numerical results of the lock-release current (line) for the cross-sections $f(z) = z^\alpha$, $\alpha = 0.5, 1, 2$ (lower, middle and upper lines; online: blue, red, green).

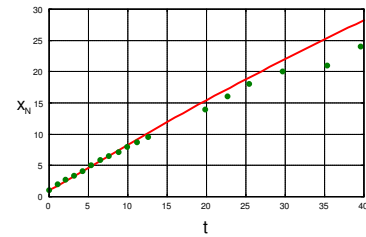


Fig. 12. Comparison of the experimental results of Monaghan et al. [3] (symbols) and SW prediction (line) for $H = 1$, $f(z) = z$.

VI. COMPARISON WITH EXPERIMENTS

It is of course desirable to corroborate the theoretical predictions of the SW model with experimental results. To our best knowledge, the only pertinent available experimental results for non-rectangular cross-sections, of [3], [4], [5], are for full-depth lock ($H = 1$) configurations. It is known from the classical rectangular case that the $H = 1$ lock-release produces some special effects which are not captured by the one-layer model (in particular, a backward-moving jump of the interface, and a long slumping interval). This is because the return flow in the ambient plays a significant role. The experiments of [3] used a tank with V-shaped bottom of 5m length, 0.4m high and 0.28m wide; the slope of inclined side-walls ($f = z$) was 25° from the horizontal. A gate was located at 0.13m from the rear of the channel. Behind the gate, the container was filled with the aqueous saline solution, while its second part contained fresh water. The initial height of the both fluids was the same ($H = 1$). In the reported experiments the flow was initiated by rapidly lifting the gate.

Fig. 12 presents a comparison between the present SW results and experimental data reported by [3] for $H = 1.0, f(z) = z$ (experiments 7-10) concerning the position of the nose, x_N , as a function of t . The laboratory data is fairly well predicted by the SW results. During the first stage of propagation ($t \lesssim 10$), the agreement between the one-layer model and experiments is actually excellent. At later times, the observed propagation lags behind the SW predictions; however, the discrepancy is only a few percent for $t < 27$, when a significant propagation of $x_N \approx 20$ is attained. For $t > 30$ the discrepancy becomes more pronounced, and it seems plausible that viscous effects become significant at this stage (consistent with the estimates of [3]).

The SW line on Fig. 12 is very close to a straight line,

in spite of the fact that the end of the constant-speed stage is at $t \approx 8$. This is because in the $f(z) = z$ the decay of the speed with time is less pronounced than in the classical rectangular case.

The real gravity current is of course more complicated than the SW solution. The observations [3] revealed a parabolic head, and strong billows on the interface. These details are beyond the resolution and the scope of the present model. However, this may indicate that some corrections due to three-dimensional flow components, turbulence, and entrainment are necessary for a more accurate understanding of the real gravity current. Given the paucity of the available experimental data, and the lack of Navier-Stokes simulation, this remains an open question.

VII. CONCLUDING REMARKS

We considered the effect of the shape of the cross-section of the channel on the time-dependent propagation of high-Reynolds-number gravity currents. The cross-section is defined by $-f_1(z) \leq y \leq f_2(z)$, $0 < z < H$; the bottom $z = 0$ and top $z = H$ walls are straight horizontal planes; the current propagates over the bottom in direction x . We used a Boussinesq one-layer shallow-water model, closed by an analytical Fr conditions at the nose (provided by Ungarish's [6] extension of Benjamin's result). The geometry of the side walls enters the formulation via $f(z) = f_1(z) + f_2(z)$. This model admits quite general forms of $f(z)$, and realistic initial and boundary conditions. The governing equations were derived from first principles, without adjustable constants.

We focused attention on currents of fixed volume generated by lock release from rest. For a given cross-section geometry, the only free input parameter is H , the height ratio of the ambient to the lock. In general, the time-dependent motion requires numerical solution. We used a simple finite-difference code based on a Lax-Wendroff two-step method. In all the tested cases, the numerical solution of the SW model was obtained within insignificant computational effort on a simple laptop computer.

We also considered analytical solutions of the SW model. We analyzed the dam-break problem, showed that an initial slumping stage with constant speed of propagation appears for any cross-section geometry, and derived a simple formula for this speed. We also revisited the analytical self-similar solution presented in previous studies ([3], [5]). We conjectured that such solutions for non-rectangular cross-sections exist only for the power-law shape $f(z) = bz^\alpha$. We compared the analytical and numerical SW results, and found good agreement.

We illustrated the application of the SW model for various cross-section forms: $f(z) = bz^\alpha$, $f(z) = b(d+z^\alpha)$ and circle segment.

REFERENCES

- [1] J. E. Simpson. *Gravity Currents in the Environment and the Laboratory*. Cambridge University Press, Cambridge UK, 1997.
- [2] M. Ungarish. *An Introduction to Gravity Currents and Intrusions*. Chapman & Hall/CRC press, Boca Raton London New York, 2009.
- [3] J.J. Monaghan, C.A. Mériaux, H.E. Huppert, and J.M. Monaghan. High Reynolds number gravity currents along V-shaped valleys. *European Journal of Mechanics - B/Fluids*, 28(5):651 – 659, 2009.
- [4] B. M. Marino and L. P. Thomas. Front condition for gravity currents in channels of nonrectangular symmetric cross-section shapes. *Journal of Fluids Engineering*, 131(5):051201, 2009.
- [5] B. M. Marino and L. P. Thomas. Dam-break release of a gravity current in a power-law channel section. *Journal of Physics: Conference Series* 296 (2011) 012008, doi: 10.1088/1742-6596/296/1/012008, 2011.
- [6] M. Ungarish. A general solution of Benjamin-type gravity current in a channel of non-rectangular cross-section. *Environ Fluid Mech.*, 12(3):251–263, 2011.
- [7] T. B. Benjamin. Gravity currents and related phenomena. *J. Fluid Mech.*, 31:209–248, 1968.
- [8] T. Bonometti, M. Ungarish, and S. Balachandar. A numerical investigation of constant-volume non-Boussinesq gravity currents in deep ambient. *J. Fluid Mech.*, 673:574–602, 2011.
- [9] M. Ungarish and T. Zemach. On the slumping of high Reynolds number gravity currents in two-dimensional and axisymmetric configurations. *European J. Mech. B/Fluids*, 24:71–90, 2005.
- [10] R. T. Bonnecaze, H. E. Huppert, and J. R. Lister. Particle-driven gravity currents. *J. Fluid Mech.*, 250:339–369, 1993.
- [11] D. Takagi and H. E. Huppert. The effect of confining boundaries on viscous gravity currents. *J. Fluid Mech.*, 577:495–505, 2007.
- [12] T. Zemach and M. Ungarish. Gravity currents in non-rectangular cross-section channels: Analytical and numerical solutions of the one-layer shallow-water model for high-Reynolds-number propagation. *Phys. of Fluids.*, 25 026601, 2013.